DOI: 10.1002/ ((please add manuscript number))

Article type: Full Paper

Graphene multi electrode arrays as a versatile tool for extracellular measurements

Dmitry Kireev, Silke Seyock, Johannes Lewen, Vanessa Maybeck, Bernhard Wolfrum,

Andreas Offenhäusser*

D. Kireev, S. Seyock, J. Lewen, Dr. V. Maybeck, Prof. A. Offenhäusser

Institute of Bioelectronics (PGI-8/ICS-8), Forschungszentrum Jülich, 52425 Jülich, Germany

E-mail: a.offenhaeusser@fz-jueluch.de

Dr. B. Wolfrum

Neuroelectronics, IMETUM, Technical University of Munich (TUM), Germany & BCCN

Munich, Boltzmannstr. 11, 85748 Garching, Germany

Keywords: graphene, GMEA, extracellular recordings, neuron

Abstract

Graphene multielectrode arrays (GMEAs), presented in this work are used for cardio and

neuronal extracellular recordings. The advantages of the graphene as part of the

multielectrode arrays are numerous: from a general flexibility and biocompatibility to the

unique electronic properties of graphene. The devices, used for extensive in vitro studies of a

cardiac-like cell line and cortical neuronal networks, show excellent ability to extracellularly

detect action potentials with signal to noise ratios in the range of 45±22 for HL-1 cells and

48±26 for spontaneous bursting/spiking neuronal activity. Complex neuronal bursting activity

patterns as well as a variety of charastic shapes of HL-1 action potentials are recorded with

the GMEAs. This paper illustrates that the potential applications of the GMEAs in biological

and medical research are still numerous and diverse.

1. Introduction

Mammalian organisms are very complex systems, which operate via even more complex

biochemical reactions. In order to understand their function and behavior, one must

understand individual cellular activities. Luckily for mankind, the most important organs – the

brain and heart - consist of electrogenic cells. This allows electrical investigation of their

1



activity. While the details, peculiarities and functions of the cells are different, the basis of the electrical activity in both cases is ion flow through the cellular membrane. Such ionic flow generates extracellular potential changes. The extracellular potentials are in the range that modern electronics already has the ability to detect accurately. Therefore, a new research field at the convergence of biology and electronics has been developed, bioelectronics. [1] Electrophysiology, as a part of bioelectronics, studies the electrical properties of biological cells and tissues (from single cells to organs). The electrophysiological recordings obtained are used in order to study cell function, understand cellular malfunctions in the diseased state, and to find ways to mimic healthy cell functions for the treatment of diseases.

One main electrophysiology tool is the planar microelectrode array (MEA). [2-3] The MEAs are traditionally used for a variety of in vitro studies from different biological cells and tissues. [4-7] The devices are usually fabricated on rigid substrates and based on metals. [3] The MEAs' performance was studied for decades, and many modifications in the composition, topography, and structure have been made. [8,9] Planar gold, titanium, and platinum, are the most commonly exploited electrode materials.^[10-15] As a further matter, it became clear that decreasing the electrode's impedance would improve the recording performance. Since they became widespread in the electrophysiological community, many interesting approaches and devices have appeared: from simple increase of roughness (via electrodeposition, [14] or use of porous metals^[12,16]), to the approach of increasing the cell-device coupling (nanocavity electrodes, [17,18] and micro 3D electrodes). [19,20] 3D structures have been pursued because not only can shapes be designed that cells can try to engulf, increasing seal resistance, but the increased material decreases the impedance of the electrode. Further development came from the use of new materials. The carbon-based nanomaterials such as carbon nanotubes (CNTs), [21,22] black carbon, porous carbon, etc. have been implemented for the fabrication of MEAs and raised interest due to their simplicity, biocompatibility, and excellent electrical properties.^[23-25]



Graphene, another allotrope of carbon, [26] has gained attention from scientists in various fields since 2004. [27] Starting with the field effect in graphene for electronic devices, it expanded into the adjacent fields of biology and bioelectronics. [28,29] In the field of electrophysiology, graphene has gained influence in cellular interfacing and signal recording. [30-32] Graphene can be used either actively as a transistor's active area, [33] or passively as an electrode. [34,35] While the graphene transistors require at least two electrical contacts per channel and a complicated read-out system, graphene multi electrode arrays (GMEAs) require just one contact per channel and the amplification system uses simpler electronics. Moreover, the GMEAs are comparably easy to fabricate, characterize, and use. The simplest graphene-based probe was reported to successfully record in-vivo heart and brain activity in 2013.^[36] However, such a device had just one very large recording electrode. This lacked the required resolution to analyze activity in a tissue. A year later, two separate works were published that both focused on local transparency of the graphene. The transparency is a great improvement compared to conventional metal-based electrodes, because it allows observation of the culture right at the recording site. The coordination of electrical activity with calcium imaging and even in vivo optogenetics is therefore possible.^[34,35]

In contrast to the above-mentioned trend towards 3D electrodes, where microstructures are designed for cells to engulf, graphene devices use the atomic monolayer structure of carbon to have a 2D electrode with exceptional in-plane conduction and sensitivity to the surrounding environment. The combination of the graphene's excellent electronic properties and its pure flatness can be exploited to outperform the 3D structured electrodes. This is possible by reducing the bulk material effects of the electrode. Considering the latest research, graphene might be a superior MEA material in some important specific subsets of neuronal interfacing. [32,37,38] For neuronal interfacing, when the axonal sizes are sub-micron, it is easier to form a good coupling with the graphene surface rather than engulf a 3D



electrode. Tension in the axon limits bending, so passing over a flat electrode allows more of the axon to be in close contact with the sensor. Moreover, graphene's transparency is an advancement compared to classical MEAs, allowing direct on-electrode monitoring of cellular viability. [35] In this work, we applied graphene for fabrication of the classic MEA elements and then implement them for the study of classic electrogenic cell cultures: the cardiac-like cell line HL-1, and the more complex cortical neuronal cultures. The overall simplicity of the fabrication process, together with the wafer-scale approach results in cheap and easy-toproduce devices. The GMEAs have detected numerous different activities from multiple HL-1 cultures. The complex cortical neuronal networks have been shown to be nicely recorded with our GMEAs, resulting in a huge number of extracellular activities with different spike shapes, amplitudes, and patterns. Low noise recordings, combined with good coupling, allow us to detect cardiac extracellular activity with signal-to-noise ratios (SNRs) up to 116 and neuronal bursting activity with SNRs up to 100 (45±22 for HL-1 cells and 48±26 for neurons. mean±standard deviation). The experiments prove the applicability of the truly twodimensional material, graphene, for the complex job of electrophysiological recordings from networks of cells. Robustness of the devices has been shown via multiple recordings from different cellular types and cultures using the same set of devices. This shows that such GMEAs are versatile tools for a general in vitro electrophysiology and a promising tool for future in vivo electrophysiology.

2. Results and discussion

The graphene multielectrode arrays are fabricated on a 4-inch wafer using CMOS-based technology. Borofloat glass and SiO₂/Si substrates were used for the device fabrication. Silicon-oxide wafers were used since they allow an extensive optical check of the fabrication steps, especially allowing visualization of graphene monolayers.^[39] Borofloat wafers were



used due to their transparency, which (a) helps to monitor the long-term cell cultures; (b) complements graphene's transparency.

The complete fabrication steps are described in the experimental section and Supporting Figure S1. In Figure 1a the schematics of the final electrode are given. The Ti/Au metal stack is used for feedlines. The feedlines have an apperture at the place where graphene (CVD-grown) electrodes are patterned. HD-8820, a photostructurable polyimide, is used for passivation. Each wafer results in 9 chips, 24×24 mm each (Figure 1b), with a 1.4×1.4 mm array of 64 electrodes in the middle (Figure 1c). From the 64 electrodes per chip, only 58 are graphene-based. Out of the 9 chips, four are with graphene electrode openings of 10 μm diameter, and five with openings of 20 μm diameter. An optical picture of a fabricated SiO₂/Si-based GMEA device is given in Figure 1d, and Figure 1e shows a chip after encapsulation (see experimental section). In order to show transparency, the same devices are fabricated on borofloat substrates, see Figure 1f for an optical picture of such devices.

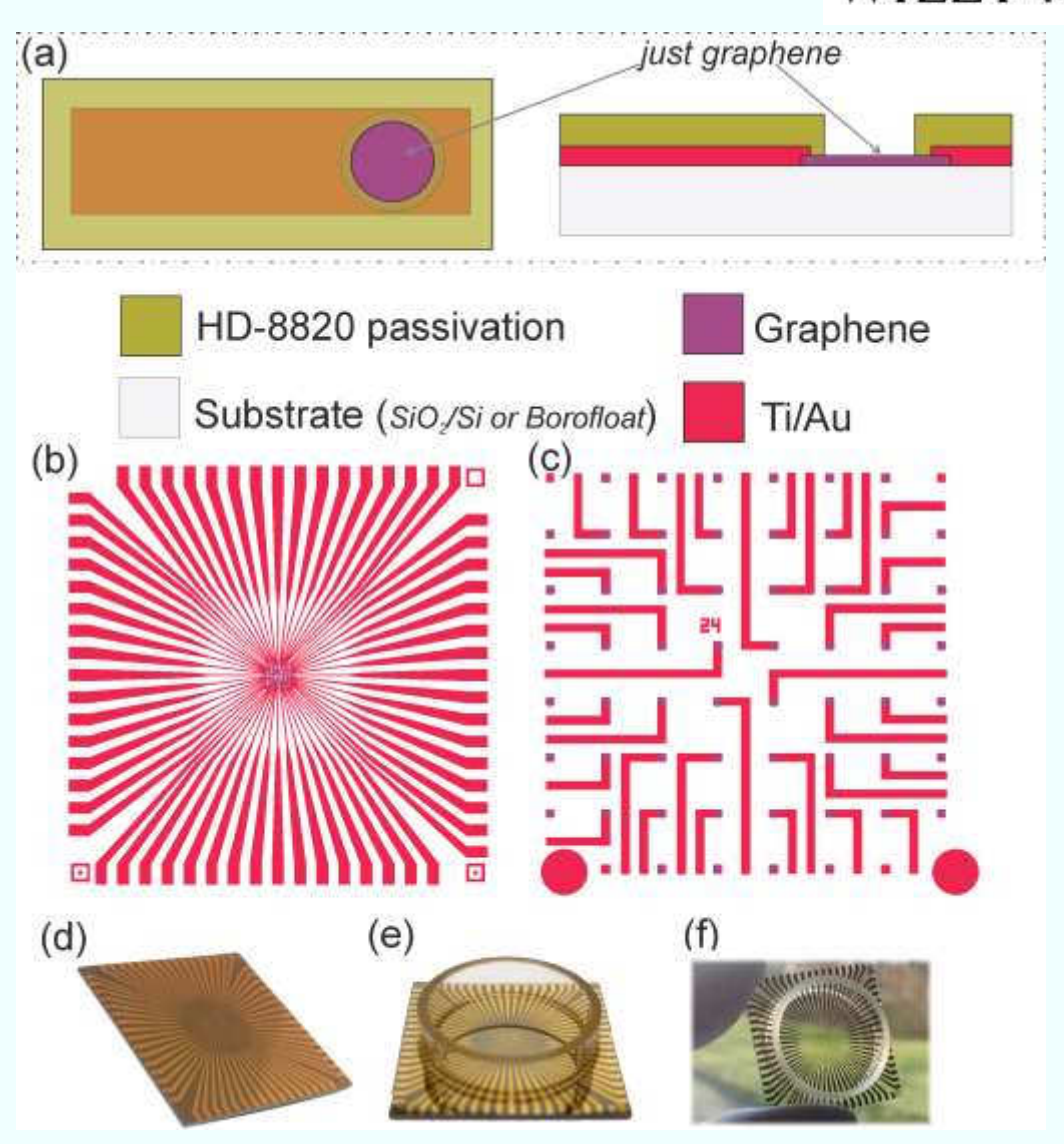


Figure 1. Fabrication overview. (a) Top and side views of a schematic of one graphene electrode. (b) The design of a GMEA chip, 24×24 mm in size. (c) Enlargement of the middle electrode array, of 1.4×1.4 mm in size. (d) An optical image of the fabricated GMEA chip (on SiO₂/Si substrate). (e) An optical image of the SiO₂/Si-based GMEA chip after encapsulation. (f) An optical image of the borofloat-based GMEA chip after encapsulation.

The GMEAs were analyzed using impedance spectroscopy (see Figure 2). In comparison to gold electrodes of the same dimensions (where 40 μ F/cm² is expected), [40] the graphene-based electrodes exhibit similar impedance: for 10 μ m electrode openings the interface capacitance is estimated to be 32±1 pF (~31.4 pF for Au); for 20 μ m it is 104±1 pF (125.7 pF for Au). Parasitic effects through the 3 μ m thick passivation (polyimide, ϵ_r =2.94) would amount to approximately 8.5 pF that have to be subtracted from the impedance values shown above. As seen from Figure 2, the impedance values are comparably large (3-4 M Ω at



1 kHz), however they are in the range of previously reported impedance values in the literature.^[34,35]

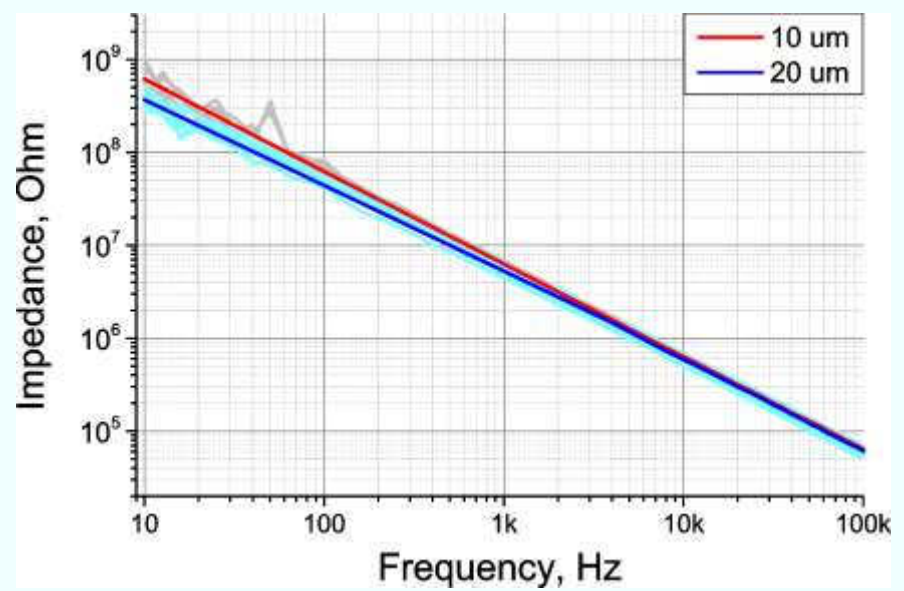


Figure 2. EIS of the 10 and 20 µm diameter GMEAs. Gray, individual traces from seven 10 µm diameter electrodes. Red, average of gray traces. Light blue, individual traces from eight 20µm diameter electrodes. Dark blue, average of light blue traces.

After encapsulation (see experimental section), the chips were used for monitoring cellular activity. Firstly, the cardiomyocyte-like cell line HL-1 was cultured on top of the encapsulated chips. HL-1 was chosen since it is commonly used as a test culture. The cells divide once per day and once confluent mature via the formation of gap junctions into a contractile tissue (see Figure 3a). Such a confluent layer starts to contract (beat) with corresponding electrical action potentials (APs) propagating through the layer via the gap junctions. The cardiac APs have an intracellular amplitude up to 150 mV peak to peak.^[41] The extracellular potentials are generally one to two orders of magnitude lower, and reach several millivolts (see Figure 3b).^[8,18,42]

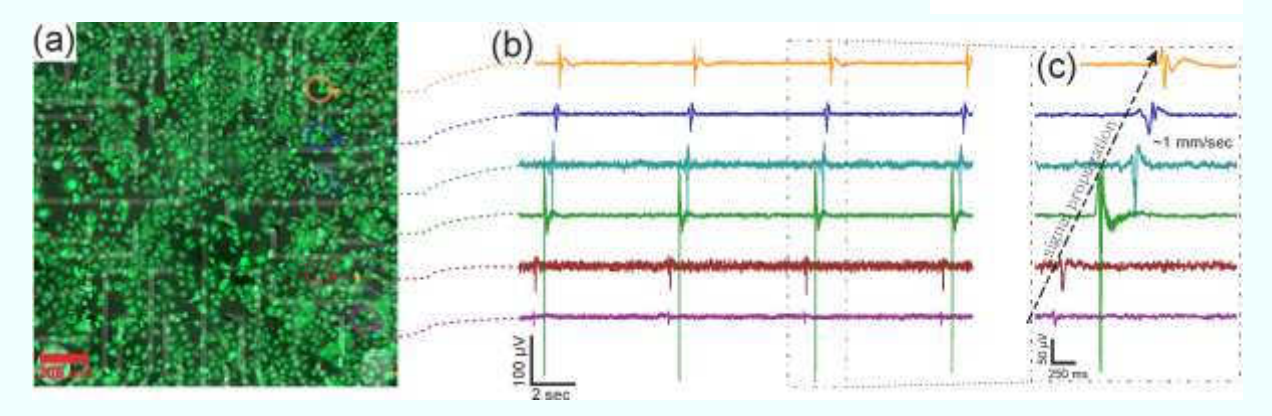


Figure 3. (a) A picture of a calcein/ethidium homodimer stained HL-1 culture on a GMEA chip. Live cells fluoresce green, dead cells fluoresce red. (b) Timetraces recording from different channels from one GMEA chip, showing the repetitiveness of the spikes and clear propagation of the signal. The color code corresponds to the electrodes circled in (a). (c) Zoom into one AP, showing propagation over the channels.

The multichannel measurement set-up (details in the experimental section) allows us to measure the whole chip in parallel. An example of the simultaneously recorded timetraces is given in Figure 3b. The clearly visible delay between APs on different channels in Figure 3bc means that: (i) the spikes are not a measurement artifact and that the channels are not crosstalking with each other (each of which would result in simultaneous spikes on multiple channels), and (ii) the signal propagates through the cell layer. [43-45] The propagation velocity and map can be deduced from the timestamps of the action potentials and corresponding geometry of the channels, as shown in Figure 3c. An examplary signal propagation is illustrated in supporting Figure S3, where a more complicated propagation is shown with multiple AP waves propagating across a single chip. This can occur if two pacemaker cells with a relatively slow beat rate are present in the same culture. The electrode to electrode pitch is 200 µm, and the propagation velocity in this case is calculated to be in the range of 1 mm/sec, which is a comparably low, but nevertheless possible value. [31,42,45,46] The beating frequency we observed was in the range of 1 ± 0.5 Hz differing from culture to culture, which is understandable beat frequency is affected by such parameters as maturity of the culture, environmental temperature and drug exposure. [47,48]



The recorded action potential amplitudes and their shapes vary from chip to chip (culture effect) and from electrode to electrode (sealing effect). [8] Over 13,000 HL-1 action potentials from 104 recorded timeseries (complete chip arrays) were analyzed. Spikes were compared to each other and to simulated data.^[8,46,49-53] Regardless of the impedance of the electrode itself, there are other physical and physiological parameters that affect the way the signal will be recorded. First of all, the more mature the culture, the larger and more stable the APs are. [54] Second is the sealing. Sealing between the cell layer and the electrode is probably the most important factor to focus on. [49] We performed comprehensive analysis and spikesorting of the 104 timeseries. From the 104 timeseries, there are a total of 595 individual timetraces (one channel) with successfully recorded APs. Due to the level of spontaneous activity, cell connectivity, and surface coverage there was a high variability in the number of timetraces extracted per timeseries. The total number of time traces per total number of time series is therefore not a measue of the number of working electrodes per chip. For further analysis, we operate on the assumption that the signal shape produced by a cell and its coupling to a specific electrode does not significantly change during one measurement. Therefore, APs detected in one timetrace should not differ significantly. This resulted in 116 unique culture-chip-electrode timetraces that could be used for spike shape analysis. The final shape distribution can be found in Figure 4a, with types A and B forming the majority (see supporting Figure S4 for the full spectrum of the spikes). According to previously simulated data, [49] spikes of type A have a large seal resistance, large sodium peak, and a large amplitude. The spikes of type A occurred in almost a third of the recorded APs. The differences in pre- and post-spikes, their amplitude, and duration can be modeled by junction resistances and current flows of Na⁺, Ca²⁺, and K⁺ ions. [49,55,56] Spikes of type B, C, and D are all variants of a triphasic shape, while differences in the post and pre-spike overshoot can be described by differences in sealing. In particular, with less sealing some ion flow may be leaking through the gap resistance and is therefore not detectable. The last type, E, which was

the rarest, has a very slow negative component that according to previously reported data can be attributed to the Ca²⁺ component of the action potential.^[55] The "other" types of spikes, mostly consist of very uncertain shapes, such as double or triple peaks, and usually are the result of a pinhole in the passivation or other defects that result in the combination of more than one AP signal on a timetrace.

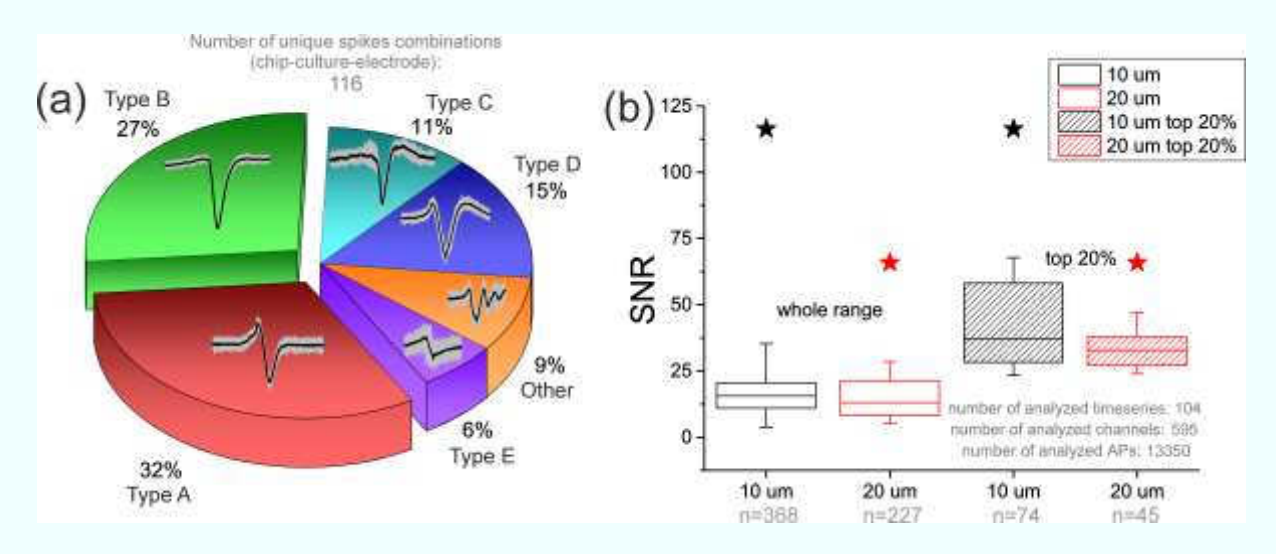


Figure 4. The result of analysis of over 13k recorded APs. From 595 channels with recorded AP trains, 116 unique combinations (culture-chip-channel) were selected and the shapes of the APs were analyzed. In (a) the prevalance of each spike type is shown. (b) gives the statistics of SNR separated according 10 and 20 μm diameter channels, box = quartiles, bar = median, whiskers = standard deviation, star = maximum value. It shows that in general there is no obvious difference between the devices, except if only top 20% of the APs are analyzed. The top 20% have been selected by taking the largest 20% of peak to peak signal amplitude values and extracting their SNRs. Also, the maximum value of the SNR is higher for the smaller devices.

Signal to noise ratios of the recordings were analyzed for each channel (n=595). The noise values (twice the median average distribution (2×MAD), see supporting Figure S5 for details) were extracted for each channel, as well as the average action potential amplitude (peak-to-peak) for the calculations. After that, the data was grouped according to the electrode diameter, and the statistical SNR values were calculated separately for small (10 μ m) and large (20 μ m) electrodes. The noise values for the two electrode types, surprisingly do not vary too much (10.26±4.8 μ V for small and 10.7±7.2 μ V for large electrodes), which could be



attributed to either the effect of quantum capacitance from the graphene,^[57,58], or to general noise restrictions due to thermal noise.^[59] As recently reported, the impedance of the graphene electrodes can be modeled via distribution of finite RC elements along the graphene-electrolyte surface.^[60] Moreover, since CVD-grown graphene is multi-crystalline, there is a higher chance of having a grain boundary in the electrode opening for the large devices, resulting in a large variation in the impedance. Additionally, in the case of larger electrodes, there is a larger area of passive graphene, which is covered with protective passivation layer, providing additional passive resistance and noise (see Supporting Figure S6).

The average SNR for 10 µm electrodes is 20±15, and for 20 µm electrodes is 17±10. The variation is very large, presumably due to variations in the culture and the coupling. In particular, we did not group detected APs according to the cell shape and position on the electrode. In order to present the performance in the best case scenario of coupling, culture health, and cell position, the top 20% of signals are presented in a separate analysis. These were selected by taking the highest 20% of peak to peak AP values. Interestingly, the signal to noise ratio of the selected 20% recordings, is larger for the small electrodes (45±22), compared to the large electrodes (35±12) (See Figure 4b and Table 1). We attribute such behavior to the fact that a smaller electrode has a better chance of a good sealing, which will improve the value for the SNR ratio by increasing peak to peak AP values. For the small electrodes we have encountered SNRs up to 116, while for large electrodes SNRs were only up to 65. We would like to point out that only a 50 Hz comb filter was applied to the recorded signal in order to remove power line hum but keep the signal as undisturbed as possible. For the details of data acquisition electronics see the experimental section.

Further, rat embryonic cortical neurons were cultured with a density of 800 cells/mm² (200k per chip with 17.8 mm inner diameter of the ring). The neurons were kept in the incubator until the culture formed a well connected network (DIV21-25). See Figure 5a for an example of a dense neuronal network on a GMEA chip. On DIV 21-25, the culture was

mature enough to produce spontaneous electrical activity throughout the network. At this point the measurements were performed. As introduced by Droge et al. in 1986, neural activity is made of spikes that can occur in bursts. One criteria for defining bursting is that the interburst intervals should be a factor of 3 larger than the interspike intervals and bursting involves correlated but non-identical spiking on multiple channels. The usual spontaneous spiking-bursting activity recorded with our GMEA chips is visible in Figure 5b, where 8 channels from one chip detected bursting activity that propagated through the network. Different kinds of bursting patterns have been recorded, and can be found in the supporting Figure S7. In our case, typical bursts happen every 5 to 15 seconds, depending on the culture, resulting in a small series of very high amplitude spikes (sometimes up to 800 μ V) followed by a series of evanescent spikes which is in agreement with the definition given above. The results are in accordance with previously published data. [4,15,62-65] In between the bursting, most of the channels have some non-bursting APs of smaller amplitude (50-150 μ V).

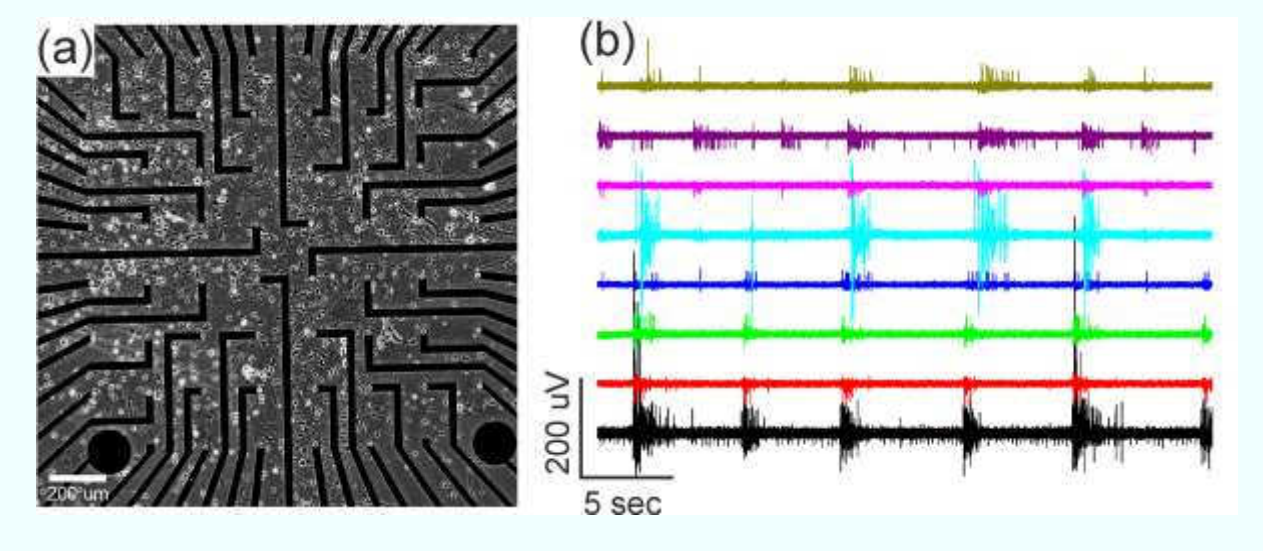


Figure 5. (a) Microscope image of the neuronal culture on a GMEA chip. (b) A timeseries recording showing excellent spiking-bursting activity on different channels. Note: the culture in (a) is different from the recording in (b).

It is difficult to follow the propagation of the neuronal signal in a comprehensive way, since the networks are complex and random, compared to the electrical syncytium of HL-1 cells. Moreover, the signal may pass through multiple neurons between two recording points.

The signal delay is then a combination of the propagation velocity through a single neuron and the synaptic delay encountered each time the signal is transferred from cell to cell.^[66,67]

In Figure 6a, a 70-second long timeseries is shown from one channel with recorded spontaneous bursting-spiking activity, with bursting patterns that happen approximately every 10 seconds. Every such burst (Figure 6b), consists of three quick spikes with large amplitude (over 300 µV, see Figure 6c), followed by a series of quickly diminishing spikes. Following the definition, the recording in Figure 6a can be described as bursting. In between the bursts, there is some non-bursting random activity (see Figure 6d). The patterns, as well as number and frequency of the bursting and non-bursting spikes vary from culture to culture. In Figure 6e four typically observed AP shapes from another culture are shown. The red bi- and triphasic forms are the average of 30 individual APs and are the most commonly observed general shape for non-bursting APs.

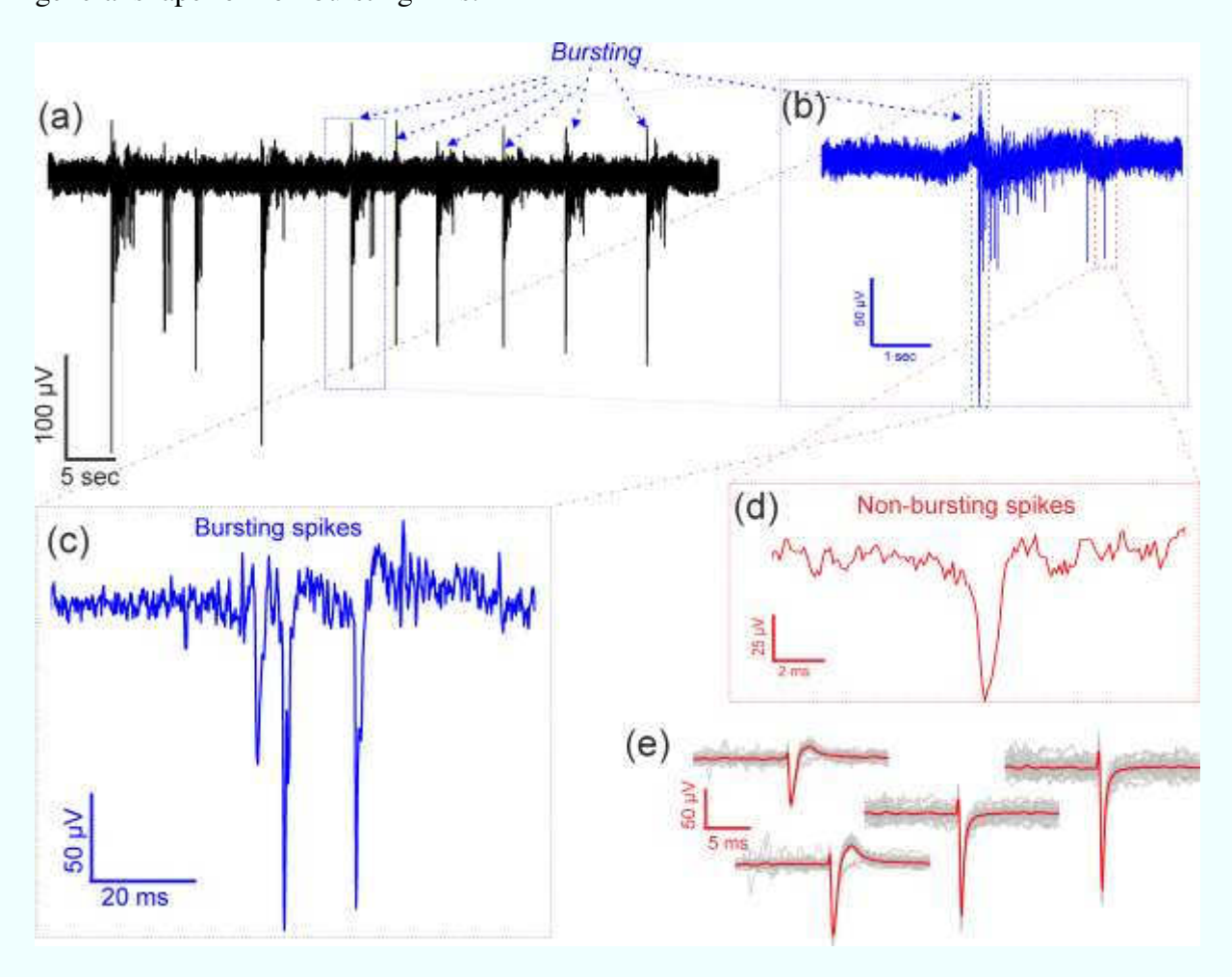




Figure 6. (a) A typical neuronal recording from a single channel, with clear repetitive spike-bursting activity; (b) is a zoom into one of the patterns, showing that each time there is a small number of very large spikes (c), followed by a series of spikes with gradually decreased amplitude. In (d) a single non-bursting spike is given. In (e) the various typical forms of non-bursting spikes are given. Extracted APs (n=30 for each) from another chip than shown in (a) are shown in gray and their average shown in red.

The variations in the shape and amplitude of the recorded neuronal APs is much larger than HL-1 spikes.^[52,68,69] This can be explained by the fact that now it is not only coupling and device performance that influence the recording, but also the morphology of the neurons: it is important to distinguish between APs detected from a soma, neurites, axons, or their combinations (if the electrodes are larger than one feature).^[70] Of course, the larger the electrode, the larger the chance to record something, but the smaller the ability to distinguish where the signal actually comes from.

Lastly, in order to prove the biological origin of the signals, we have conducted a series of chemical experiments. We treated the cultures on different chips with different chemicals that are established in the literature to induce/reduce the firing rate, or even kill the whole culture. Sodium dodecyl sulfate (SDS), potassium chloride (KCl), and Tetrodotoxin (TTX) were used for this purpose. We would like to point out that the experiments were not performed as specifically designed drug tests, but rather as a proof of principle that the GMEAs are able to record the effects and the devices continue to function after the treatments.

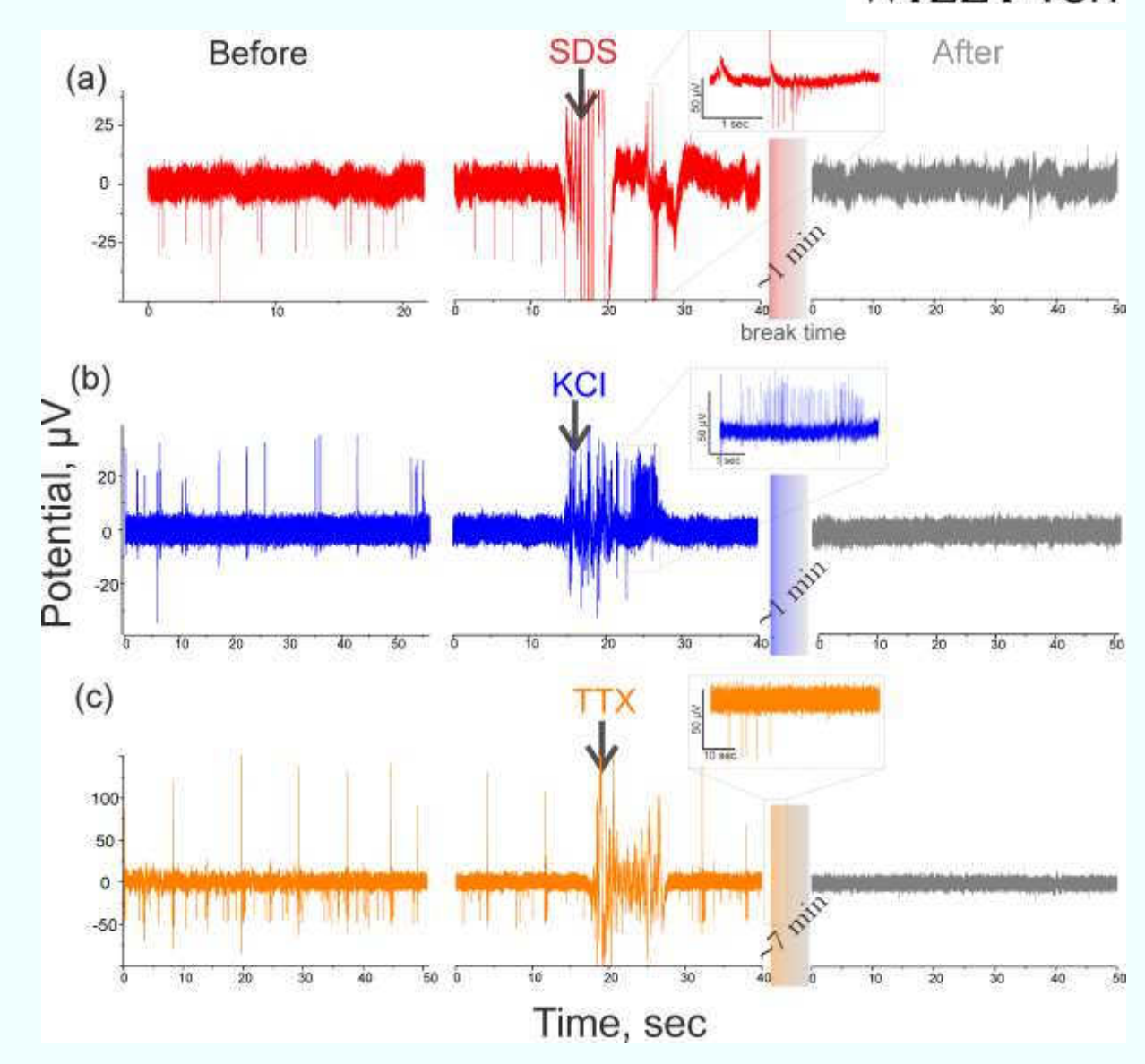


Figure 7. Chemical treatments of the neuronal networks with SDS (a), KCl (b) and TTX (c). The left panels are the recordings before any treatment. The large signal fluctuations in the recordings in the middle panels are from addition of the chemicals and is due to mechanical perturbations and a slow mixing (pipetting in/out) of the liquid to distribute the substance evenly to the cells. The right panels are recordings 1 minute (for SDS and KCl), and 7 minutes (for TTX) after the treatments. In the middle are the 40 seconds of the timetraces when the chemical was added into the medium. Small instets show the immediate effects when the chemicals alter the normal neuronal bursting-spiking activity.

The effect of the above-mentioned chemicals on neuronal cultures was observed in real-time measurements with the GMEAs (see Figure 7). SDS, a surfactant, permeabilizes the cell membrane and dissolves cell material from the surface. Exchange of 50% of the supplemented medium with a saturated solution of SDS resulted in a fast (<20 seconds) and irreversible detachment of the cellular layer and cessation of detected spikes (see Figure 7a).



In another culture, potassium chloride was added to the medium to reach a final concentration of 10-20 mM. This elevation of extracellular potassium concentration depolarizes the cell. Such an extracellular concentration is enough to depolarize the cell above threshold and prevent repolarization (see Figure 7b). This results in the cells firing and then remaining in depolarization block. As seen in the fluorescent live-dead picture afterwards (see supporting Figure S8) the cells survive this treatment, in contrast to the SDS where cells are removed. TTX, on the other hand, is a neurotoxin which blocks Na_v channels. Upon addition to the cell culture, at a concentration of ~0.7 μ M, the AP amplitude, as well as spiking frequency slowly decreases as the toxin binds to more and more channels preventing their function, until no more signals are seen (Figure 7c). The effect of TTX on the activity is different (faster'slower) for different timetraces (electrodes), which refelects the complexity of the whole neuronal network. The timeseries recordings for all channels exposed to TTX are given in the supporting Figure S9.

At the end we would like to point out two important issues. First, the same GMEAs were used to record several cultures of HL-1 cells (>10, 3-4 DIV each) and several cortical neuronal cultures (>5, 14-25 DIV each) with a cleaning step (in 1% (w/v) terg-A-Zyme) in between. The quality of the electrodes does not seem to be deteriorated by the cultures or cleaning, proving the stability of the devices. Second, all the values of SNR and AP amplitude presented above were calculated using limited noise filtering. Only 50 Hz noise and its harmonics together with linear slopes were removed by post-processing. Further filtering can disturb the actual shapes of the potential, but could theoretically improve all SNR values by 30-40%. Moreover, we would like to argue at this point that such orthodox device schematics (with an opening in passivation that forces the neurons to bend inside) is not an optimal way to implement graphene's truly two-dimensional structure. Therefore, in order to better match the graphene's properties, a better design can be sought that brings graphene onto the same



level as the passivation or thin the passivation down to nanometer scale, possibly with the use of other 2D materials.

Table 1. Comparison of the noise and SNR values to the state-of-the-art.

	Active material	Substrate	Electrode diameter	$\begin{array}{c} \text{Noise level}, \\ \mu V \end{array}$	SNR HL-1 cells	SNR neuronal
This work	Graphene	SiO ₂ /Si and Borofloat	10 μm	10.26±4.8 ^{a)}	45±22 b) (max - 116)	
			20 μm	10.7±7.2 ^{a)}	35±12 ^{b)} (max - 65)	Bursting: 48±26(max – 100) Spontaneous: 16±6 (max – 33)
Du et al. ^[71]	Graphene	Quartz	20 μm	15±5		10.3±1.2
Bruggemann et al.[12]	Au planar	SiO ₂ /Si	10 μm 20 μm	7 6.5	57 ^{c)} 141 ^{c)}	
Kim et al.[13]	Au flakes	Glass	5-50 μm			20±10
Hofmann et al.	Au nanocavity	SiO2/Si	10 μm	9.5±0.5 ^{c)}	158±8	
James et al.[14]	Au/Pt	Fused silica	12 μm	15±5 ^{d)}		15±10
Berdondini et al. ^[15]	Pt	SiO ₂ /Si Pyrex7740	30 μm 22 μm	8.2 6.5		N/A

a) Estimated as 2×MAD; b) Calculated from the top 20% of the recorded data; c) Estimated as 1×RMS;

3. Conclusions

In conclusion, the graphene-based MEAs presented show excellent properties, which have been used for extracellular recordings. HL-1 cells, as well as neuronal networks, have been recorded *in vitro* via the same GMEAs, showing excellent SNRs of 45±22 for cardiac and 48±26 for neuronal bursting activity. To our knowledge, this is also the first time spontaneous neuronal spiking-bursting activity is recorded by graphene-based electrodes *in vitro*.

Although it is already possible to clarify that the graphene-based electrodes result in very stable recordings from different kinds of cells, there is still room for improvement of the GMEAs. In the manuscript we have proven the potential application of the GMEAs for recording cardiac and neuronal activities. Moreover, the general flexibility, transparency,

d) Estimated as peak-to-peak values.



biocompatibility, ease of fabrication and usage of graphene make it a promising material for a more advanced neuronal interfacing, such as in brain and retina implants.

4. Experimental Section

GMEA fabrication: Silicon wafers (p++) with 285 nm of silicon oxide and borofloat wafers were used as the substrates for further fabrication. The first metallization of Ti and Au was done in order to fabricate alignment markers. Further, the CVD grown graphene was transferred onto the wafer by the high-throughput transfer technique described previously.^[72] Afterwards, an AZ5214 photoresist, spin-coated at 3000 rpm, soft-baked at 110°C, exposed with a dose of 55 mJ/cm² and developed in 0.26% TMAH solution for 70 seconds, was used to protect graphene active areas during oxygen plasma treatment (300 W power, 200 sccm for 5 minutes). The 10 nm Ti and 90 nm Au metallization stack was deposited via e-beam assisted evaporation on the wafer with a pre-defined structure of LOR-3B (3000 rpm, softbaked at 150°C for 5 minutes) and nLOF-2020 (3000 rpm, soft-baked at 100°C for 2 minutes exposed with a dose of 40 mJ/cm², and developed in 0.26 % TMAH for a total of 33 seconds). For passivation, a photostructurable polyimide, HD-8820 (HD Microsystems), was used. Polyimide was spin-coated at 5000 rpm, soft-baked at 120°C for 4 minutes (slow ramp), exposed with a dose of 250 mJ/cm², and developed in 0.26% TMAH for approximately 80 seconds, then hard-baked with a slow ramp up to 350°C for 30 minutes (4°C/min up to 200°C, followed by 2.5°C/min up to 350°C), followed by slow cooling, to form a pinhole free, 3 µm thick passivation.

Chip encapsulation: In order to perform cell cultures on the chips, the samples were encapsulated by attaching a glass ring with an outer diameter of 20 mm (17.8 mm inner diameter) on top of the 24×24 mm chip using PDMS (10:1, Sylgard). The glass ring is 4 mm tall, which provides approximately 1 mL volume for the culture medium. Prior to the cell culture, the chips were cleaned with running DI water, then sterilized with 70% ethanol and



transferred into the sterile bench. There, the chips were functionalized with cell-specific proteins.

HL-1 culture: For the culture of the adherent cardiomyocytes, fibronectin and gelatin (5 μg/mL and 0.2 mg/mL) in double distilled water was used as the coating for the chips. The samples were coated for 1h at 37°C, then washed with phosphate-buffered saline (PBS) solution. Afterwards, the cells were seeded with a concentration of 100-200 cells/mm² and were cultured for 3 to 4 days in a humified incubator at 37°C and 5% CO₂ until a confluent layer formed. The growth state was monitored via a light microscope. The Claycomb medium supplemented with 10% fetal bovine serum (FBS), 100 U/ml-100 μg/ml penicillin-streptomycin (Life Technology), 0.1 mM norepinephrine, and 2mM L-glutamine (Life Technology) was exchanged every day and two hours before the measurements.

Impedance spectroscopy: Electrical impedance spectroscopy was performed on a multichannel potentiostat, VSP-300 (BioLogic Science Instruments). The measurements were performed using graphene as a working electrode and a Ag/AgCl pellet as a reference electrode. The spectra were taken in a frequency range from 10 Hz to 100 kHz in 1x PBS solution, while a 10 mV AC potential was applied. The interface capacitance is calculated using a simplified Randles circuit.

Multichannel recordings: The recordings were performed within two hours of removing a chip from the incubator. There were neither special temperature nor other environmental controls while measuring. The recordings were performed on the home-built amplifier system, BioMAS, with 64-channel recording, allowing a maximum amplification of 1010 (10.1×1×10×100). All 64 channels are sampled simultaneously with a sampling rate of 10 kHz. Additionally, there is an 3 kHz anti-aliasing low-pass is installed in the amplifier system. A Ag/AgCl pellet (Warner Instruments) was used as a reference electrode. The recording was controlled via LabView based software and the analysis was done via MATLAB.



Spike sorting and SNR calulations: Prior to analysis of the recordings, a 50 Hz comb filter was applied to the recorded timeseries in order to remove power line hum but keep the signal as undisturbed as possible. Peak-to-peak signal amplitude, as well as noise values, were calculated for each timetrace individually and used to determine the SNR values for each timetrace. The noise analysis was performed on a whole timetrace (without artificial and manual selection of interspike intervals), therefore RMS values, as visible from Supporting Figure S5, are not a good estimate. However, the 2×MAD values were found to be the most accurate estimate of the actual peak-to-peak noise. From the unique culture-chip-electrode timetraces, the 116 action potentials (see Supporting Figure S4) were extracted extracted as 200 ms segments centered on the highest amplitude peak of the waveform, averaged, plotted, and lastly sorted manually.

Neuronal culture: For the culture of embryonic neurons the samples are coated with a mixture of 0.01 mg/mL poly-D-lysine (PDL), 0.004 mg/mL gelatin, and 0.1 mg/mL extracellular matrix in Gey's Balanced Salt Solution (GBSS). The coating is applied for 1 h at room temperature and afterwards washed off using GBSS. Primary cortical neurons were prepared from E18 Wistar rats.^[73] The neuronal cells were seeded on top of the samples with a concentration of 800 cells/mm² and after 1 hour the medium, consisting of Neurobasal medium (Life Technologies) supplemented with 1% (v/v) B-27 (Gibco), 0.5 mM L-glutamine and 0.05 mg/mL Gentamicin, was exchanged. The cells were cultured for 21–25 days in a humidified incubator at 37°C with 5% CO₂. Half of the medium was exchanged twice a week and two hours before the measurements. Right before the measurements, the neurobasal medium was exchanged with extracellular patch (E-patch) solution, containing 120 mM NaCl, 3 mM KCl, 1 mM MgCl₂, 10 mM Hepes, 2 mM CaCl₂, matched with glucose to the osmolarity of the medium as measured immediately before the experiment.

Chemical treatments: A saturated KCl (350 mg/ml) and a TTX (250 µM) solution were prepared in a deionized (DI) water in advance and added directly into 1 ml of E-patch



medium during the recordings to reach the final concentration of 10-20 mM for KCl, and 0.7 μM for TTX. SDS, on the other hand, was dissolved in DI water up to its solubility limit (200 mg/mL), and the E-patch solution was replaced by SDS solution during the measurements. *Live-dead imaging:* The cells were labeled with Calcein AM, (1 μg/ml, Life Technologies) and Ethidium Homodimer (2 μM, Life Technologies) for 15 minutes at 37°C. Afterwards, the solution was replaced with fresh PBS. The cells were observed using fluorescent microscopy. If not stated otherwise, all chemicals are purchased from Sigma Aldrich. The experiments are done with the approval of the Landesumweltamt für Natur, Umwelt und Verbraucherschutz Nordrhein-Westfalen, Recklinghausen, Germany, number 84-02.04.2015.A173.

Supporting Information

Supporting Information is available from the Wiley Online Library or from the author.

Acknowledgements

We are grateful to Tianru Wu for graphene growth and Bettina Breuer for neuronal preparations. The work was supported by Helmholz-CAS JRG funding.

Received: ((will be filled in by the editorial staff))
Revised: ((will be filled in by the editorial staff))
Published online: ((will be filled in by the editorial staff))

- [1] G. M. Walker, J. M. Ramsey, A Framework for Bioelectronics Discovery and Innovation, https://www.nist.gov/sites/default/files/documents/pml/div683/bioelectronics_report.pdf
- [2] C. A. Thomas, G. E. Loeb, L. M. Okunj, *Exp. Cell. Res.* **1972**, 74, 61
- [3] P. Wang, Q. Liu, Cell-Based Biosensors: Principles and Applications, Artech House, Norwood, USA, 2009.
- [4] G. W. Gross, A. N. Williams, J. H. Lucas, J. Neurosci. Methods 1982, 5, 13.
- [5] U. Egert, B. Schlosshauer, S. Fennrich, W. Nisch, M. Fejtl, T. Knott, T. Müller, H. Hämmerle, *Brain Res. Protoc.* **1998**, 2, 229.
- [6] T. Neumann, C. Ziegler, A. Blau, *Brain Res.* **2008**, 1207, 120.
- [7] A. Natarajan, P. Molnar, K. Sieverdes, A. Jamshidi, J. J. Hickman, *Toxicol. Vitr.* **2006**, 20, 375.
- [8] M. E. Spira A. Hai, Nat. Nanotechnol. 2013, 8, 83.
- [9] M. E. J. Obien, K. Deligkaris, T. Bullmann, D. J. Bakkum, U. Frey, *Front. Neurosci.* **2015**, 9.
- [10] W. L. C. Rutten, Annu. Rev. Biomed. Eng. 2002, 4, 407.
- [11] U. Frey, U. Egert, F. Heer, S. Hafizovic, A. Hierlemann, *Biosens. Bioelectron.* **2009**, 24, 2191.
- [12] D. Brüggemann, B. Wolfrum, V. Maybeck, Y. Mourzina, M. Jansen, A. Offenhäusser, *Nanotechnology* **2011**, 22, 265104.
- [13] J.-H. Kim, G. Kang, Y. Nam, Y.-K. Choi, *Nanotechnology* **2010**, 21, 085303.
- [14] C. D. James, A. J. H. Spence, N. M. Dowell-Mesfin, R. J. Hussain, K. L. Smith, H. G.



- Craighead, M. S. Isaacson, W. Shain, J. N. Turner, *IEEE Trans. Biomed. Eng.* **2004**, 51, 1640.
- [15] L. Berdondini, P. Massobrio, M. Chiappalone, M. Tedesco, K. Imfeld, A. Maccione, M. Gandolfo, M. Koudelka-Hep, S. Martinoia, *J. Neurosci. Methods* **2009**, 177, 386.
- [16] F. Ceyssens, S. P. Sree, J. Martens, R. Puers, *Procedia Eng.* **2015**, 120, 355.
- [17] B. Hofmann, E. Kätelhön, M. Schottdorf, A. Offenhäusser, B. Wolfrum, *Lab Chip* **2011**, 11, 1054.
- [18] A. Czeschik, P. Rinklin, U. Derra, S. Ullmann, P. Holik, S. S. Steltenkamp, A. Offenhäusser, B. Wolfrum, *Nanoscale* **2015**, 7, 9275.
- [19] A. Fendyur, M. E. Spira, Front. Neuroeng. 2012, 5, 1.
- [20] F. Santoro, S. Dasgupta, J. Schnitker, T. Auth, E. Neumann, G. Panaitov, G. Gompper, A. Offenhäusser, *ACS Nano* **2014**, 8, 6713.
- [21] T. D. B. Nguyen-Vu, H. Chen, A. M. Cassell, R. Andrews, M. Meyyappan, J. Li, *Small* **2006**, 2, 89.
- [22] T. Gabay, M. Ben-David, I. Kalifa, R. Sorkin, Z. R. Abrams, E. Ben-Jacob, Y. Hanein, *Nanotechnology* **2007**, 18, 035201.
- [23] A. Shoval, Front. Neuroeng. **2009**, 2, 4.
- [24] M. David-Pur, L. Bareket-Keren, G. Beit-Yaakov, D. Raz-Prag, Y. Hanein, *Biomed. Microdevices* **2014**, 16, 43.
- [25] T. Kim, J. Park, J. Sohn, D. Cho, S. Jeon, ACS Nano 2016, 10, 4770.
- [26] A. Bianco, H.-M. Cheng, T. Enoki, Y. Gogotsi, R. H. Hurt, N. Koratkar, T. Kyotani, M. Monthioux, C. R. Park, J. M. D. Tascon, J. Zhang, *Carbon* **2013**, 65, 1.
- [27] K. S. S. Novoselov, A. K. K. Geim, S. V. V Morozov, D. Jiang, Y. Zhang, S. V. V Dubonos, I. V. V Grigorieva, A. A. A. Firsov, *Science* 2004,306, 666.
- [28] A. Servant, A. Bianco, M. Prato, K. Kostarelos, *Bioorg. Med. Chem. Lett.* **2014**, 24, 1638
- [29] N. Li, Y. Cheng, Q. Song, Z. Jiang, M. Tang, and G. Cheng, *Chinese Sci. Bull.* **2014**, 59, 1341.
- [30] M. Dankerl, M. V. Hauf, A. Lippert, L. H. Hess, S. Birner, I. D. Sharp, A. Mahmood, P. Mallet, J.-Y. Y. Veuillen, M. Stutzmann, J. A. Garrido, *Adv. Funct. Mater.* **2010**, 20, 3117.
- [31] L. H. Hess, M. Jansen, V. Maybeck, M. V Hauf, M. Seifert, M. Stutzmann, I. D. Sharp, A. Offenhäusser, J. A. Garrido, *Adv. Mater.* **2011**, 23, 5045.
- [32] A. Bendali, L. H. Hess, M. Seifert, V. Forster, A. Stephan, J. A Garrido, S. Picaud, *Adv. Healthc. Mater.* **2013**, 2, 929.
- [33] L. H. Hess, M. V. Hauf, M. Seifert, F. Speck, T. Seyller, M. Stutzmann, I. D. Sharp, J. A. Garrido, *Appl. Phys. Lett.* **2011**, 99, 033503.
- [34] D. Kuzum, H. Takano, E. Shim, J. C. Reed, H. Juul, A. G. Richardson, J. de Vries, H. Bink, M. A. Dichter, T. H. Lucas, D. A. Coulter, E. Cubukcu, B. Litt, *Nat. Commun.* **2014**, 5, 5259.
- [35] D.-W. Park, A. A. Schendel, S. Mikael, S. K. Brodnick, T. J. Richner, J. P. Ness, M. R. Hayat, F. Atry, S. T. Frye, R. Pashaie, S. Thongpang, Z. Ma, J. C. Williams, *Nat. Commun.* **2014**, 5, 5258.
- [36] C. H. Chen, C. Te Lin, W. L. Hsu, Y. C. Chang, S. R. Yeh, L. J. Li, D. J. Yao, *Nanomedicine Nanotechnology, Biol. Med.* **2013**, 9, 600.
- [37] A. Fabbro, D. Scaini, V. León, E. Vázquez, G. Cellot, G. Privitera, L. Lombardi, F. Torrisi, F. Tomarchio, F. Bonaccorso, S. Bosi, A. C. Ferrari, L. Ballerini, M. Prato, *ACS Nano* **2016**, 10, 615.
- [38] F. Veliev, A. Briançon-Marjollet, V. Bouchiat, C. Delacour, *Biomaterials* **2016**, 86, 33.
- [39] P. Blake, E. W. Hill, A. H. Castro Neto, K. S. Novoselov, D. Jiang, R. Yang, T. J. Booth, A. K. Geim, *Appl. Phys. Lett.* **2007**, 91, 063124.

- [40] A. J. Bard and L. R. Faulkner, *Electrochemical Methods: Fundamentals and Applications*, Wiley, **2000**.
- [41] Y. Y. Lu, Y. C. Chen, Y. H. Kao, Y. K. Lin, Y. H. Yeh, S. A. Chen, Y. J. Chen, J. Cell. Mol. Med. 2016, 20, 1182.
- [42] B. Hofmann, V. Maybeck, S. Eick, S. Meffert, S. Ingebrandt, P. Wood, E. Bamberg, A. Offenhäusser, *Lab Chip* **2010**,10, 2588.
- [43] J. P. Fahrenbach, R. Mejia-Alvarez, K. Banach, J. Physiol. 2007, 585, 565.
- [44] W. C. Claycomb, N. A. Lanson, B. S. Stallworth, D. B. Egeland, J. B. Delcarpio, A. Bahinski, N. J. Izzo, *Proc Natl Acad Sci USA* **1998**, 95, 2979.
- [45] S. M. White, P. E. Constantin, and W. C. Claycomb, *Am. J. Physiol. Heart Circ. Physiol.* **2004**, 286, H823.
- [46] V. Maybeck, R. Edgington, A. Bongrain, J. O. Welch, E. Scorsone, P. Bergonzo, R. B. Jackman, A. Offenhäusser, *Adv. Healthc. Mater.* **2014**, 3, 283.
- [47] L. Sartiani, P. Bochet, E. Cerbai, A. Mugelli, R. Fischmeister, *J. Physiol.* **2002**, 545, 81.
- [48] A. R. Natarajan, Q. Rong, A. N. Katchman, S. N. Ebert, *Pediatr. Res.* **2004**, 56, 411.
- [49] M. Schottdorf, B. Hofmann, E. Kätelhön, A. Offenhäusser, B. Wolfrum, *Phys. Rev. E Stat. Nonlinear, Soft Matter Phys.* **2012**, 85, 031917.
- [50] B. M. Blaschke, M. Lottner, S. Drieschner, A. B. Calia, K. Stoiber, L. Rousseau, G. Lissourges, J. A. Garrido, *2D Mater.* **2016**, 3, 025007.
- [51] P. Fromherz, Eur. Biophys. J. 1999, 28, 254.
- [52] P. M. Bulai, P. G. Molchanov, A. A. Denisov, T. N. Pitlik, S. N. Cherenkevich, *Eur. Biophys. J.* **2012**, 41, 319.
- [53] J. L. Puglisi, F. Wang, D. M. Bers, *Prog. Biophys. Mol. Biol.* **2004**, 85.
- [54] C. Xie, Z. Lin, L. Hanson, Y. Cui, B. Cui, Nat. Nanotechnol. 2012, 7, 185.
- [55] C. Sprössler, M. Denyer, S. Britland, W. Knoll, A. Offenhäusser, *Phys. Rev. E. Stat. Phys. Plasmas. Fluids. Relat. Interdiscip. Topics* **1999**, 60, 2171.
- [56] P. Fromherz, A. Offenhäusser, T. Vetter, J. Weis, *Science* **1991**, 252, 1290.
- [57] J. Xia, F. Chen, J. Li, N. Tao, Nat Nanotechnol 2009, 4, 505.
- [58] X. Du, H. Guo, Y. Jin, Q. Jin, J. Zhao, *Electroanalysis* **2015**, 27, 12, 2760.
- [59] M. S. Crosser, M. A. Brown, P. L. McEuen, E. D. Minot, *Nano Lett.* **2015**, 15, 5404.
- [60] S. Drieschner, A. Guimerà, R. G. Cortadella, D. Viana, E. Makrygiannis, B. M. Blaschke, J. Vieten, and J. A. Garrido, *J. Phys. D. Appl. Phys.* **2017**, 50, 095304.
- [61] M. H. Droge, G. W. Gross, M. H. Hightower, L. E. Czisny, J. Neurosci. 1986, 6, 1583.
- [62] M. Chiappalone, M. Bove, A. Vato, M. Tedesco, S. Martinoia, *Brain Res.* **2006**, 1093, 41
- [63] G. W. Gross, *IEEE Trans. Biomed. Eng.* **1979**, 26, 273.
- [64] V. Pasquale, P. Massobrio, L. L. Bologna, M. Chiappalone, S. Martinoia, *Neuroscience* **2008**, 153,1354.
- [65] J. Van Pelt, P. S. Wolters, M. A. Corner, W. L. C. Rutten, G. J. A. Ramakers, *IEEE Trans. Biomed. Eng.* **2004**, 51, 2051.
- [66] T. C. Ruch, H. D. Patton, *Physiology and biophysics*. Saunders (W.B.) Co Ltd, Philadelphia, **1982**.
- [67] E. Kandel, J. H. Schwartz, T. M. Jessell, *Principles of Neural Science*, McGraw-Hill Medical, Chicago, **2000**.
- [68] B. C. Wheeler Y. Nam, Crit. Rev. Biomed. Eng. 2011, 39, 45.
- [69] P. Massobrio, G. Massobrio, S. Martinoia, Front. Neurosci. 2016, 10, 1.
- [70] P. Fromherz, Ann. N. Y. Acad. Sci. 2006, 1093, 143.
- [71] X. Du, L. Wu, J. Cheng, S. Huang, Q. Cai, Q. Jin, J. Zhao, J. Biol. Phys. 2015, 41, 339.
- [72] D. Kireev, D. Sarik, T. Wu, X. Xie, B. Wolfrum, A. Offenhäusser, *Carbon* **2016**, 107, 319.



[73] G. J. Brewer, J. R. Torricelli, E. K. Evege, P. J. Price, J. Neurosci. Res. 1993, 35, 567.



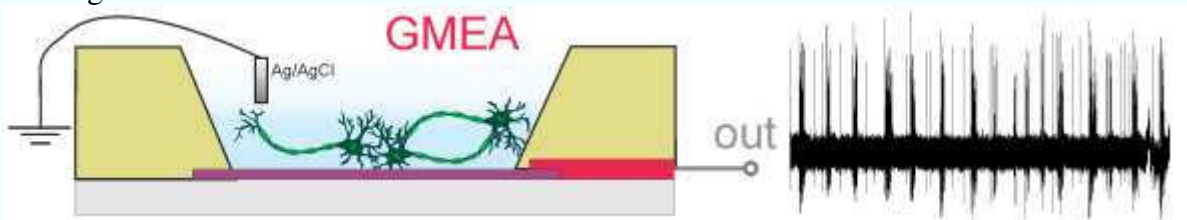
Graphene multielectrode arrays, reported in the work, exhibit exceellent ability to record electrophysiological signals. Cardiac-like cell activity, as well as complex neuronal acitivity can be recorded with the arrays of graphene-based electrodes. Low noise performance, the corresponding large signal to noise ratio, and excellent long term *in vitro* stability place the GMEAs at the forefront of electrophysiological tools.

Graphene, GMEA, extracellular recordings, neuron

D. Kireev, S. Seyock, J. Lewen, V. Maybeck, B. Wolfrum, A. Offenhäusser*

Graphene multi electrode arrays as a versatile tool for extracellular measurements

ToC figure:



Copyright WILEY-VCH Verlag GmbH & Co. KGaA, 69469 Weinheim, Germany, 2013.

Supporting Information

Graphene multi electrode arrays as a versatile tool for extracellular measurements

Dmitry Kireev, Silke Seyock, Johannes Lewen, Vanessa Maybeck, Bernhard Wolfrum, Andreas Offenhäusser*

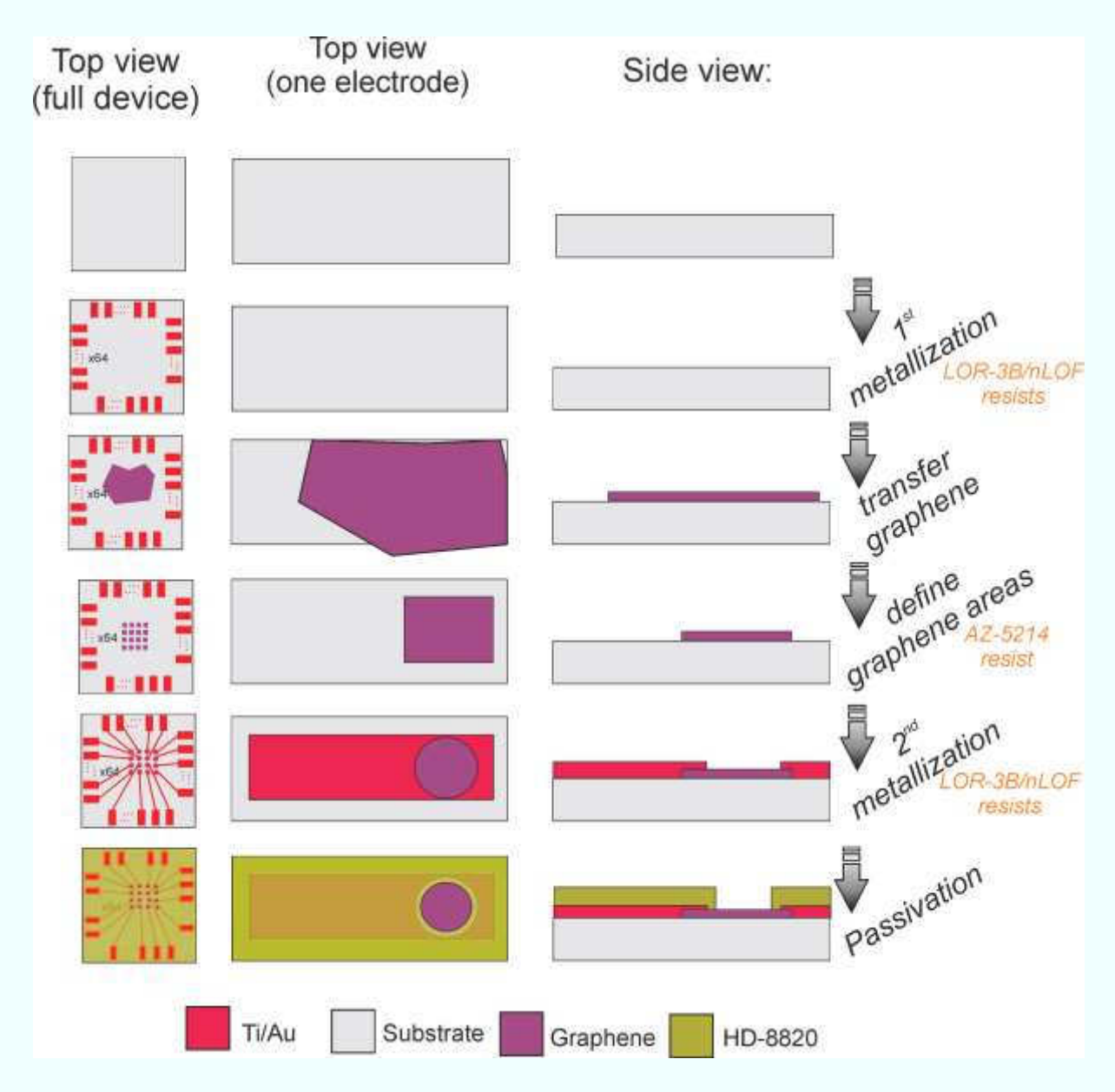


Figure S1. The detailed fabrication flow of a GMEA with three different perspectives: top view of a full device, top view of one electrode and side view of one electrode.

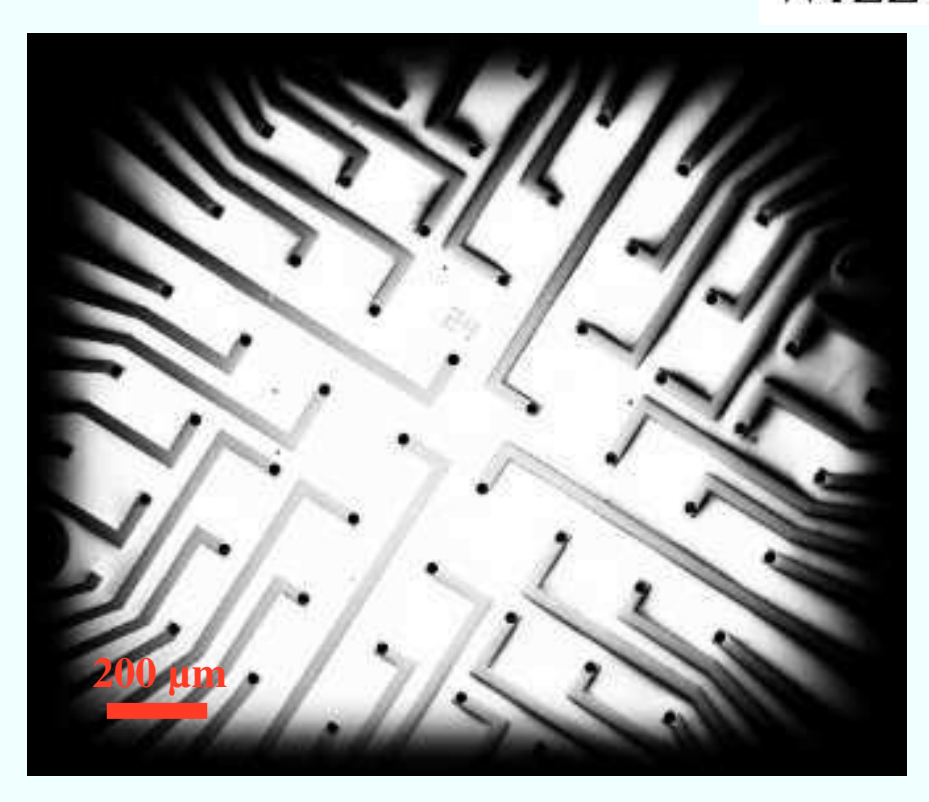


Figure S2. An SEM image of a GMEA in the fabrication step after metallization, but before passivation. The dark spots in the middle of the metal feedlines are areas of graphene.

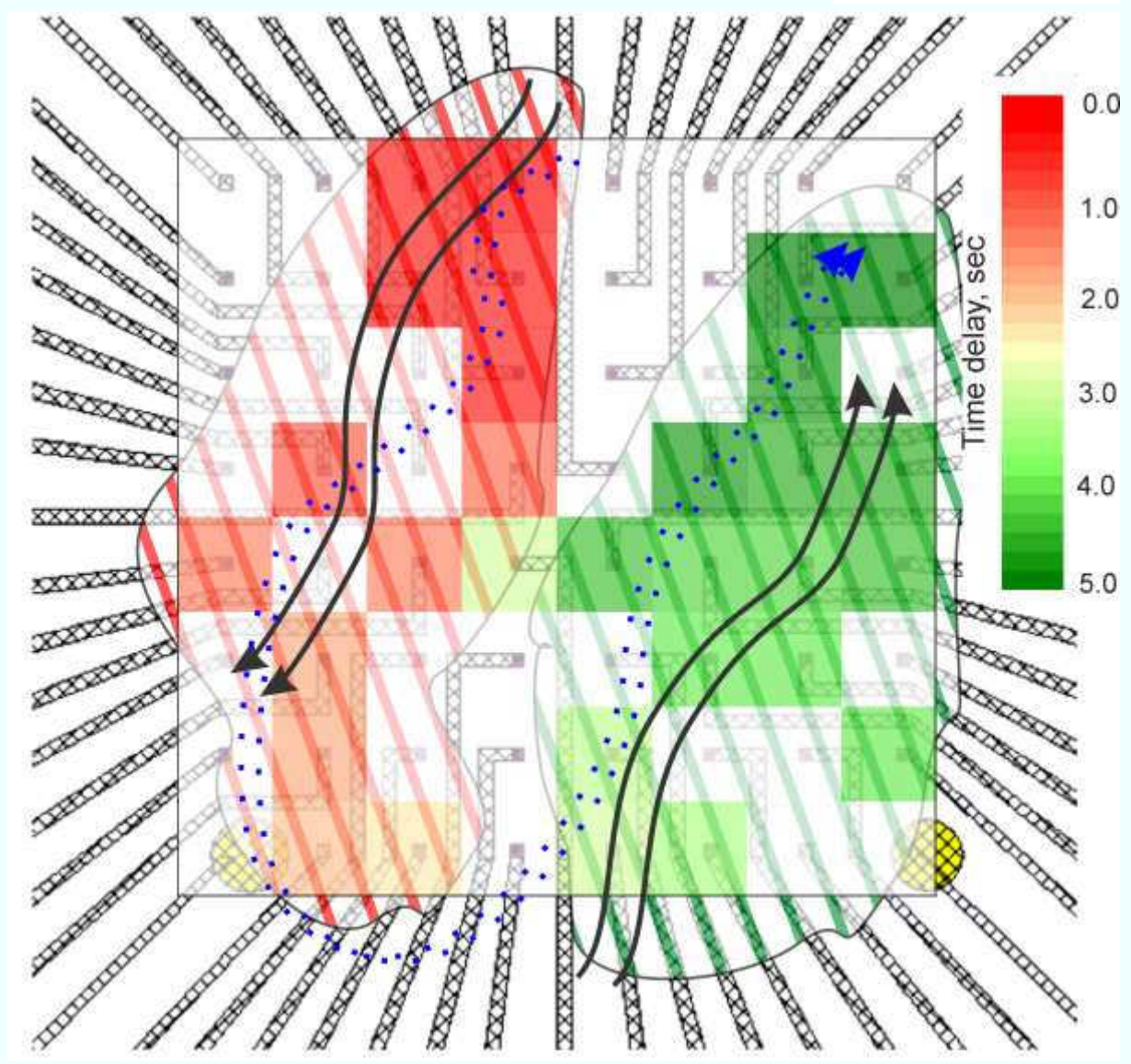


Figure S3. HL-1 signal propagation showing that either the signal is propagating in a U-shape (possibly due to reduced or lack of gap junctions in the middle of the cell layer), see blue dotted path; or there are two pacemakers, depicted as two separate black solid paths. In the latter case, the boundary between the two beating regions is located the middle of the chip, and the left side has a signal flow top to bottom, and while the right side flows from bottom to top.

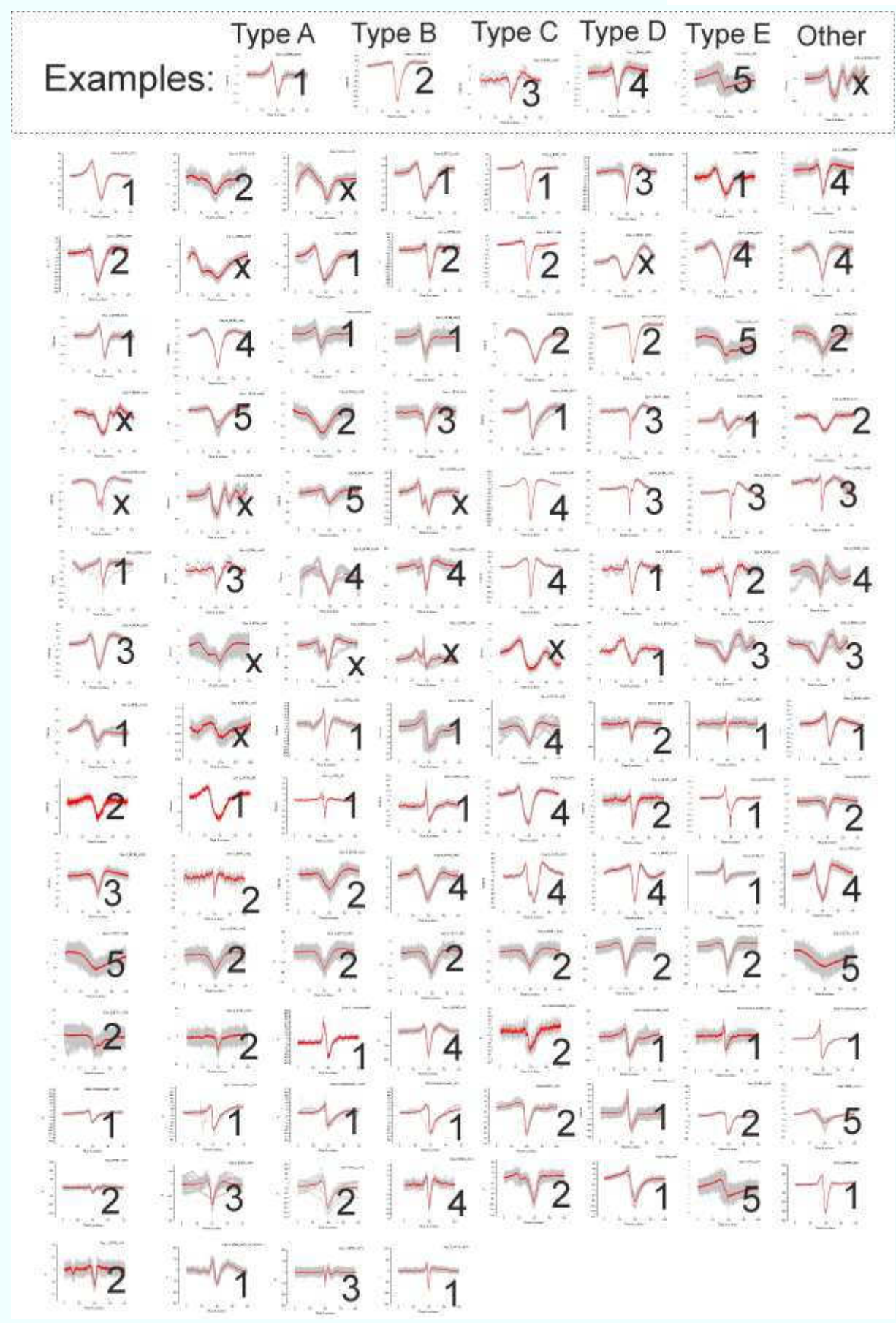


Figure S4. The variety of the HL-1 action potential spike forms recorded with the 116 unique culture-chip-channel combinations and their assigned classification.

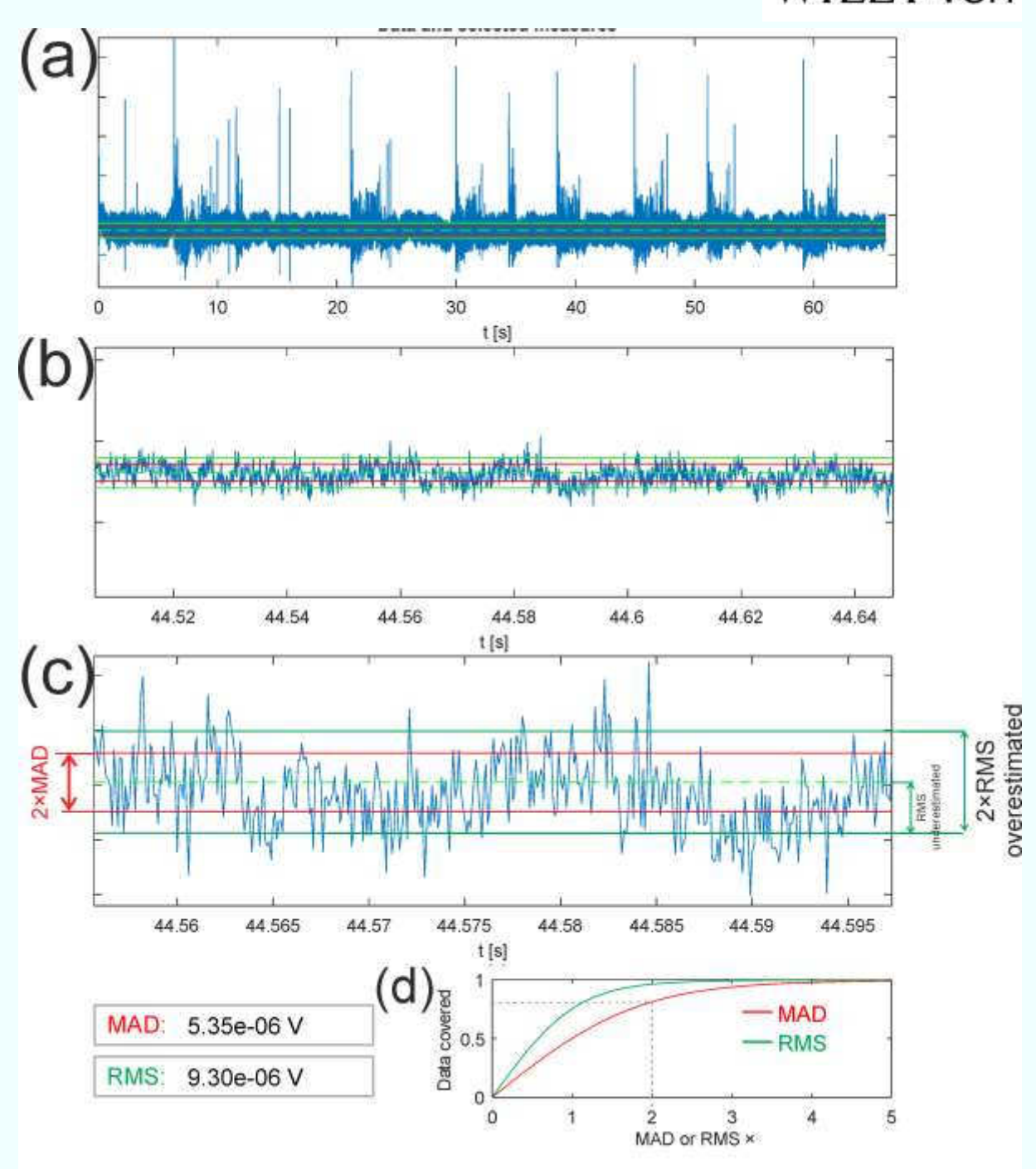
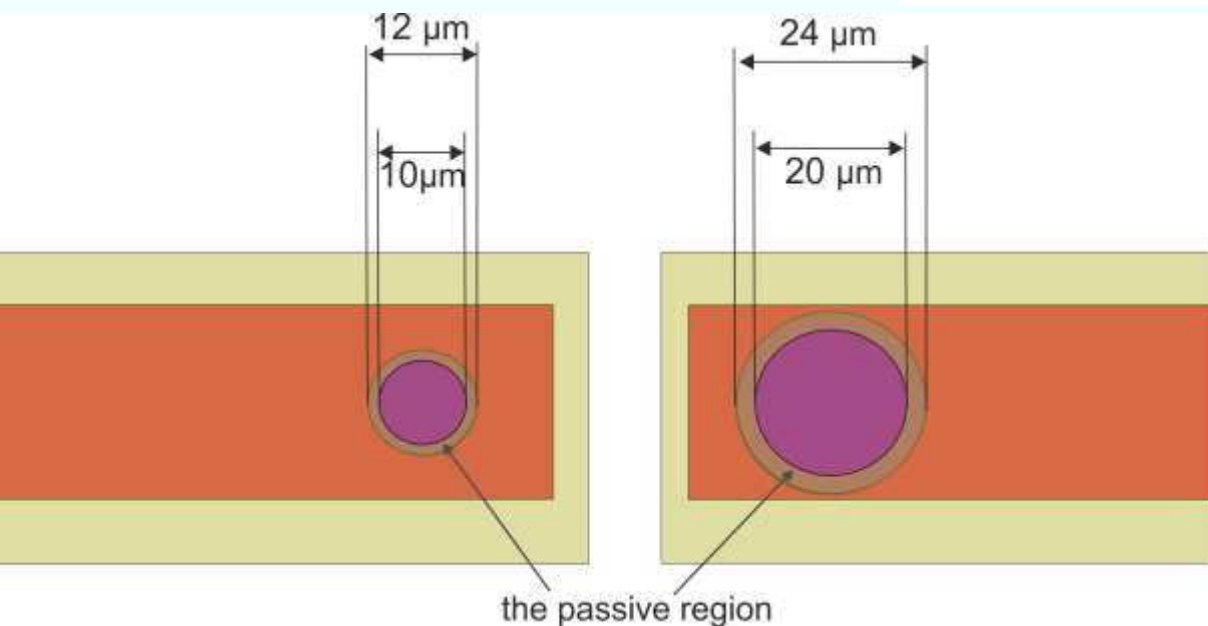
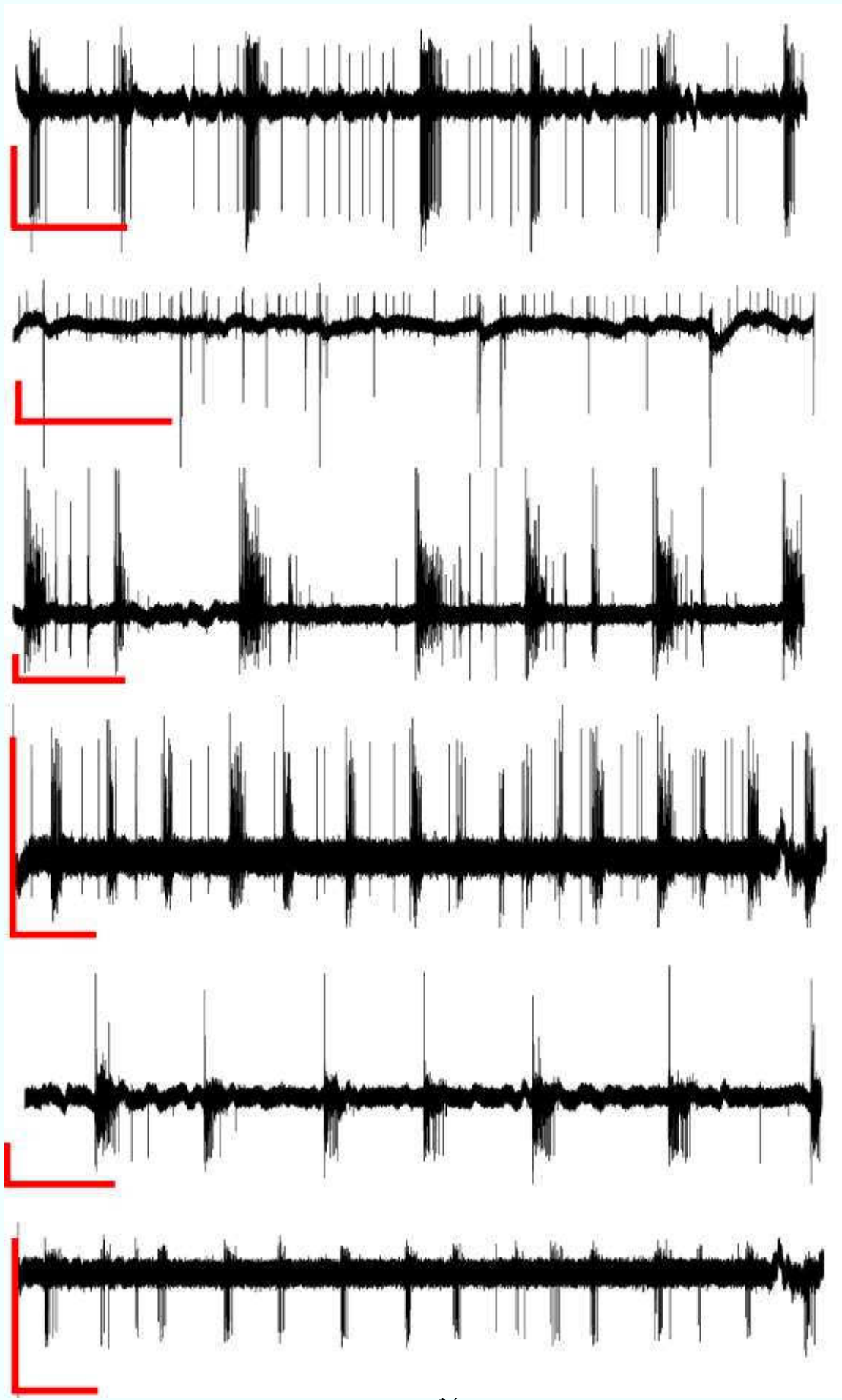


Figure S5. The discussion of MAD and RMS noise values. In (a) a 60 second long recording with bursting activity is shown. The noise analysis is done on the whole timetrace. (b) gives a 10 ms zoom into a region without spikes. In (c) is shown just 4 ms so that individual noise peaks are visible. Green horizontal lines on each trace represent the RMS values, red horizontal lines mark the MAD values. In figures (b) and (c) is easily visible that 2×RMS value is much larger than actual peak-to-peak noise. An RMS value, on the other hand is found to be slightly smaller than the peak-to-peak noise (depends on culture and amount of spikes in the timetrace). The 2×MAD values are found to represent the actual peak-to-peak noise most accurately. As shown in figure (d), around 80% of the raw data (including the spikes), is covered by the 2×MAD values. The 2×RMS values in the case cover almost 100%, which results in overestimation, since the overall timetrace with spikes is considered.



the passive region

Figure S6. A sketch of direct comparison between a 10 um and 20 um electrode device. In the larger electrodes, there is, clearle a larger area of a passive graphene, providing only additional resistance and noise, increasing the overall impedance/noise level.



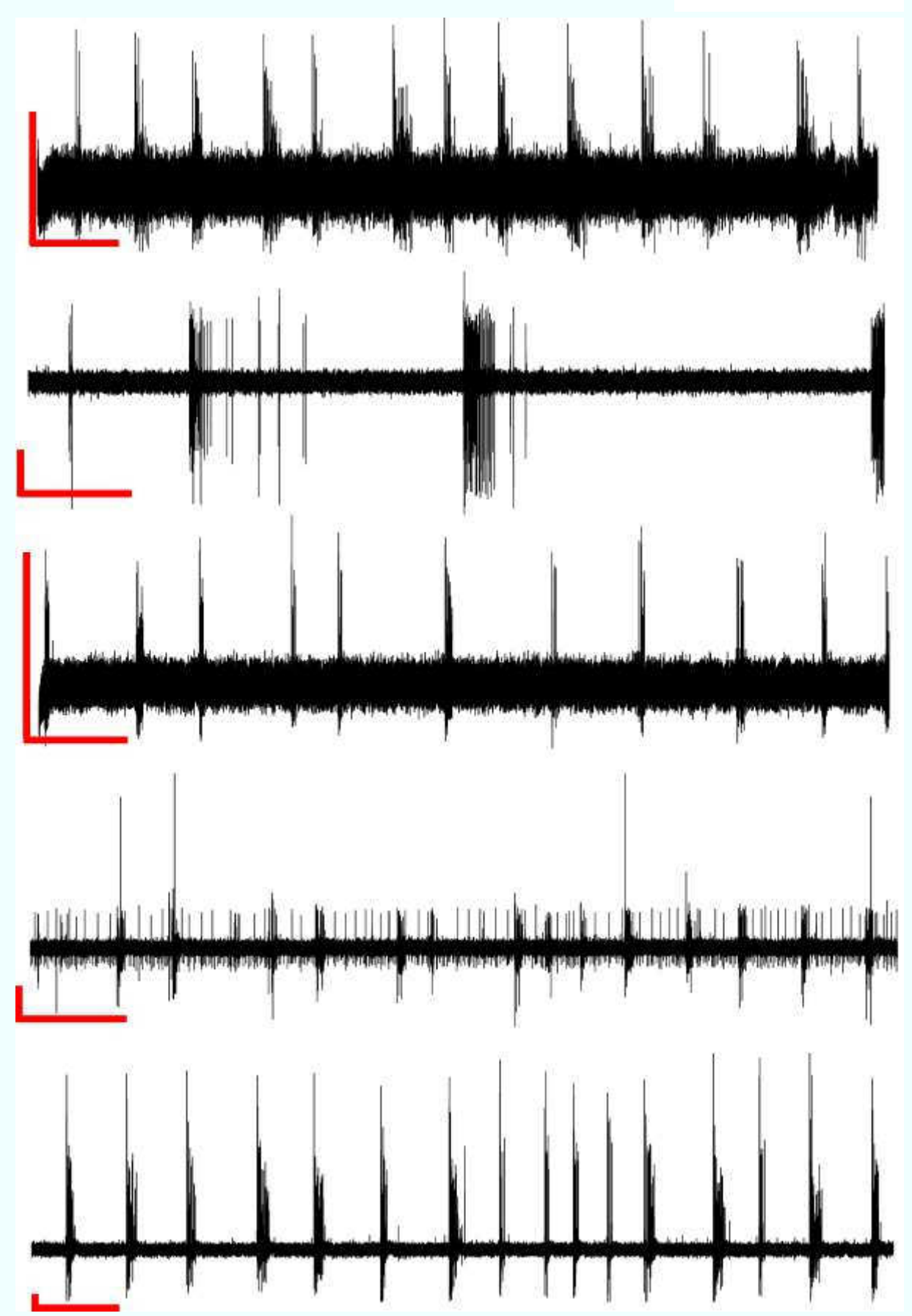


Figure S7. Some of the different patterns of bursting-spiking activity from neuronal networks recorded by the GMEAs. The scale bars given for each recording are 50 μ V on the vertical and 10 sec on the horizontal.

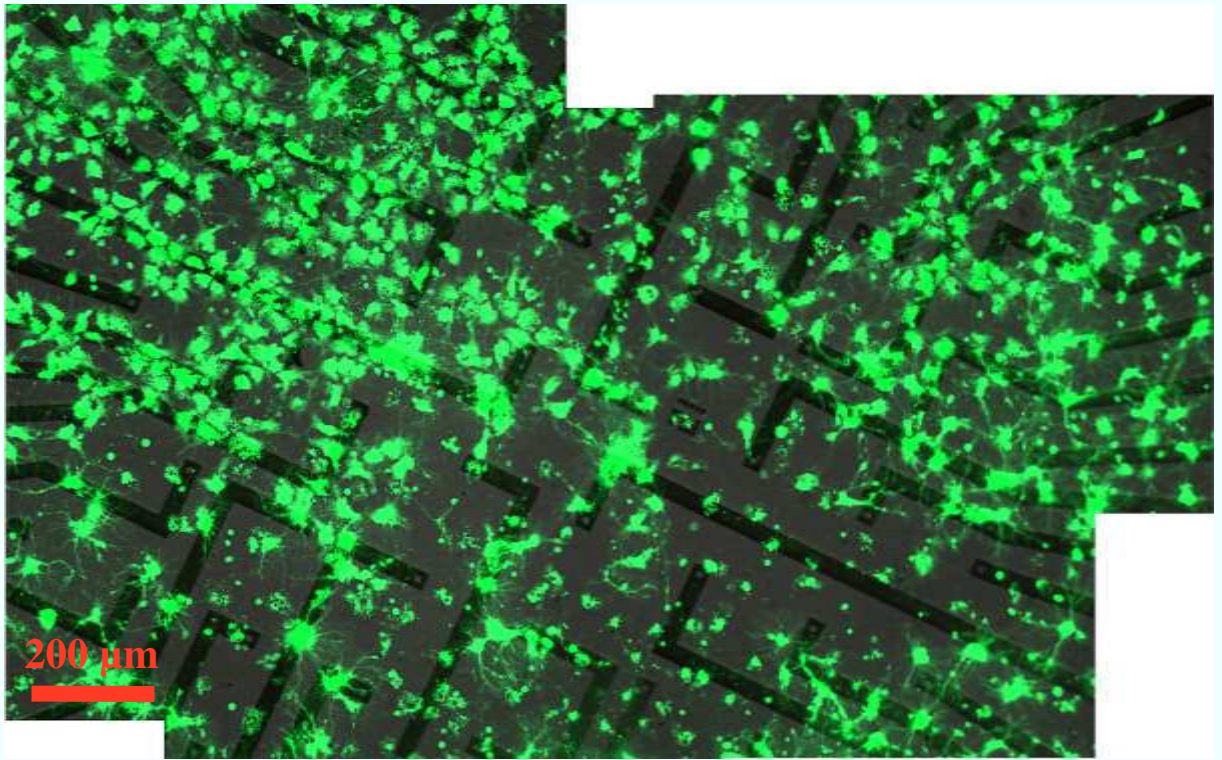
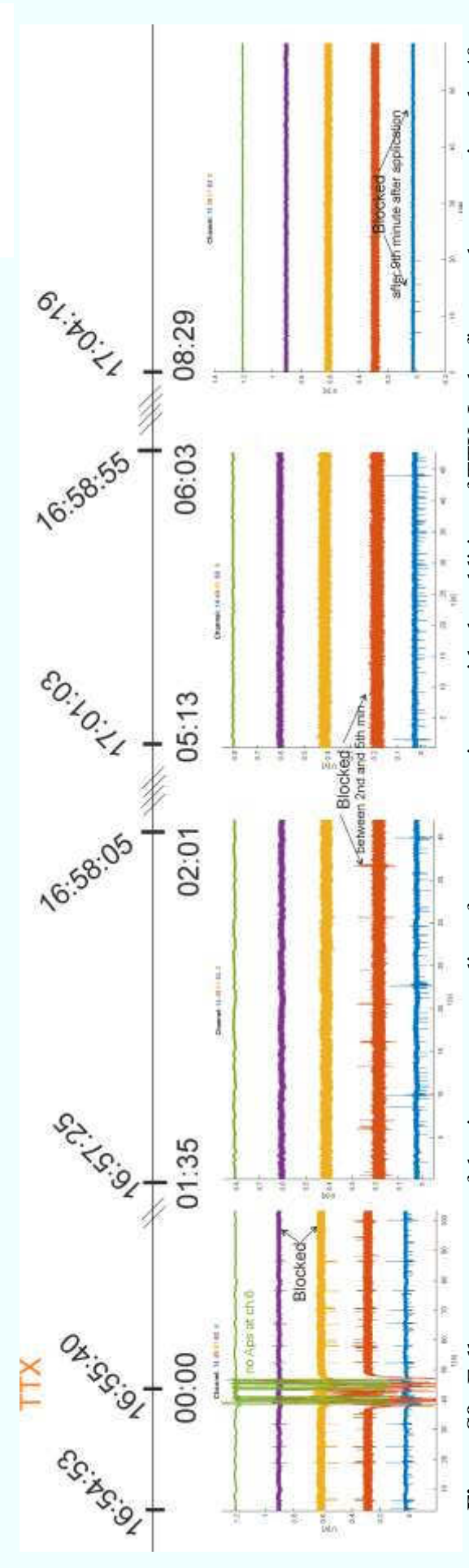


Figure S8. Live-dead panorama image of a chip after addition of 20_mM KCl



seconds from the beginning of the recordings, TTX was added to a final concentration approximately 0.7 µM. The moment when TTX was added is Interestingly, the spikings on channel #14 were dissaperaing very slowly: First the bursting frequency decreased, and the totalspiking activity stoped firing action potentials. The neurons on channel #49 stoped firing between the 2nd and 5th minute after TTX addition (no recording during this time). taken as a zero point for further time reference. Approximately 40-50 seconds after the TTX was added, two channels (#61 and #63) had stopped Figure S9. Full arrangement of the timetrace recordings from one experiment with the addition of TTX. In the first graph, approximately 40 only after the 9th minute.

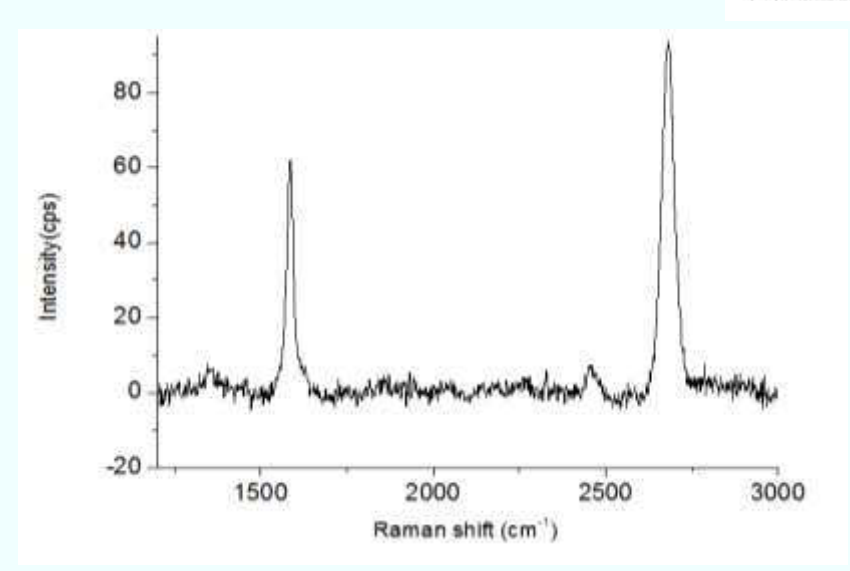


Figure S10. Raman spectra of the CVD grown graphene that was used in this work.